Site requirements and elementary steps in dimethyl ether carbonylation catalyzed by acidic zeolites

Patricia Cheung [a], Aditya Bhan [a], Glenn J. Sunley [b], David J. Law [b], Enrique Iglesia [a,*]

[a] *Department of Chemical Engineering, University of California at Berkeley, Berkeley, CA 94720, USA*
[b] *BP Chemicals, Hull Research and Technology Centre, Saltend, Hull HU12 8DS, UK*

Abstract

Steady-state, transient, and isotopic-exchange studies of dimethyl ether (DME) carbonylation, combined with adsorption and desorption studies of probe molecules and infrared (IR) spectroscopy, were used to identify methyl and acetyl groups as surface intermediates within specific elementary steps involved in the synthesis of methyl acetate from DME–CO mixtures with >99% selectivity on H-zeolites. Carbonylation rates increased linearly with CO pressures but did not depend on DME pressures, suggesting that the addition of CO to CH_3 groups present at saturation coverage controls catalytic carbonylation rates. These reactions lead to acetyl groups that subsequently react with DME to form methyl acetate (423–463 K; >99% selectivity) and regenerate methyl intermediates, consistent with kinetic studies of CO reactions with CH_3 groups previously formed from DME and with kinetic and IR studies of DME reactions with acetyl groups formed by stoichiometric reactions of acetic anhydride. These studies show that CO reacts with DME-derived intermediates bound on zeolitic Al sites from the gas phase or via weakly held CO species adsorbed non-competitively with CH_3 groups. These reactions, in contrast with similar reactions of methanol, occur under anhydrous conditions and avoid the formation of water, which strongly inhibits carbonylation reactions.
© 2006 Elsevier Inc. All rights reserved.

Keywords: Carbonylation; Acid; Zeolite; Mordenite; Dimethyl ether; Methanol; Carbon monoxide; Methyl acetate; Acetic acid; Carboxylic acid

1. Introduction

Methanol carbonylation accounts for ∼60% of acetic acid production worldwide [1–5]. The Monsanto and BP Cativa™ processes use homogeneous Rh or Ir complexes and iodide co-catalysts to carbonylate methanol (30–60 bar, 423–473 K) [1]. The Acetica process uses an immobilized Rh–carbonyl complex grafted onto a pyridine-containing solid resin and iodide co-catalysts to improve throughput and catalyst recovery [6]. Practical methanol carbonylation catalysts without costly noble metals and corrosive iodide co-catalysis remain unavailable.

Carbonylation of alkenes and alkanols to carboxylic acids via Koch-type reactions [7] is catalyzed by strong acids without metal co-catalysts [8,9]. Acidic zeolites and sulfated zirconia catalyze the carbonylation of alkanols and alkenes to

carboxylic acids via Koch-type pathways, which involve CO insertion into C–O bonds within tertiary surface-bound alkoxides and subsequent hydrolysis of the bound acetyl intermediates formed [10–16]. Fujimoto and co-workers first reported methanol carbonylation to acetic acid on zeolites and proposed an intermediate role of surface methyl groups [17]. Similar reactions of methanol and dimethyl ether (DME) were later reported on acidic zeolites and polyoxometallate clusters, but with significant homologation side reactions and catalyst deactivation [18–23]. A preliminary note from our group showed that H-mordenite (H-MOR) and H-ferrierite (H-FER) catalyzed DME carbonylation to methyl acetate with stable rates and >99% selectivity at 423–463 K after an initial induction period, during which acidic protons were replaced by methyl groups and the water co-produced was removed [24]. The rate of DME carbonylation was much higher than for similar reactions of CH_3OH, at least in part because H_2O, formed in parallel CH_3OH dehydration reactions, inhibits carbonylation steps. Methyl acetate synthesis rates did not depend on DME pressure,

but increased linearly with CO pressure up to ∼1 MPa. This kinetic response is consistent with a sequence of elementary steps involving the formation of surface methyl groups at Brønsted acid sites initially via direct DME reactions with protons and then via chain transfer reactions of DME with surface acetyls formed via rate-determining CO insertion into C–O bonds in methyl groups at the catalytic steady state [24].

Here we provide evidence for these intermediates and elementary steps and for their consistency with the measured kinetic effects of DME, CO, and H_2O using infrared (IR) spectroscopy, isotopic tracer and kinetic effects, and transient reaction studies. We also report that H-MOR samples with similar Si/Al ratio and extra-framework Al content give different carbonylation turnover rates (per H^+); methyl acetate synthesis rates on these H-MOR samples do not correlate with the number of CO binding sites measured from low-temperature CO adsorption uptakes, suggesting that the specific siting and structure of acidic Al–OH groups is critical to stabilize transition states required for kinetically relevant CO insertion steps. In the context of these results, we discuss various possible structures for such active sites, specifically those involved in formation of the C–C bond in methyl acetate synthesis.

2. Experimental

2.1. Catalyst preparation

Na-MOR (Si/Al ∼ 6.5, Zeolyst) was converted to NH_4-MOR via four sequential exchanges of Na-MOR (10 g) with 1 M NH_4NO_3 (0.2 L) at 353 K for 12 h. After each exchange, the NH_4-MOR was washed with 0.2 L of deionized water and isolated by filtration. After the final exchange, the sample was treated overnight at 393 K in ambient air and then in flowing dry air (zero grade, Praxair) for 3 h at 773 K (0.167 K s^{-1}).

Chemically dealuminated HMOR samples were prepared by refluxing HMOR (Si/Al ∼ 10, Zeolyst) in a 1.5 M aqueous solution of oxalic acid dihydrate (99%, Fluka) (catalyst:oxalic acid solution = 1:5, v/v) at 313, 323, or 343 K for 3 h before washing with (0.2 L) deionized water, filtering, and drying at 393 K in ambient air overnight; this process was carried out to remove detrital Al species, but it also removed some framework Al atoms [25,26]. The samples were subsequently treated at 773 K (0.0167 K s^{-1}) in flowing dry air (zero grade, Praxair) for 3 h. This treatment was carried out to explore the effects of Al content on DME carbonylation rates.

NH_4-MOR (Si/Al ∼ 10, Zeolyst, ∼14 g) was exchanged with Na using 0.5 L aqueous $NaNO_3$ (99%, EMD Chemicals, 0.014–2.44 M) at 353 K for 12 h and then washed in 2 L of deionized water and treated at 393 K overnight in ambient air and then in flowing dry air (zero grade, Praxair) for 3 h at 773 K (0.167 K s^{-1}). This treatment was carried out to explore the effects of replacing H^+ with Na^+ on the rate of DME carbonylation on residual protons.

NH_4-MOR (Si/Al ∼ 10, Zeolyst), H-MOR (Si/Al ∼ 44.5, Zeolyst), H-MOR (Si/Al ∼ 10, Sudchemie), H-MOR (Si/Al ∼ 9.5, Tosoh), and NH_4-MFI (Si/Al ∼ 12.5, AlSi-Penta Zeolithe GmbH) samples were treated in flowing dry air (zero grade,

Table 1
Elemental analysis and extra-framework Al content from ^{27}Al MAS NMR of zeolite samples

Zeolite name	Source	Si/Al$_{ICP}$	Na/Al$_{ICP}$	Al$_{EF}$ (%)
HMOR_8.9	Tosoh	8.9	–	20.7
HMOR_10.1	Sudchemie	10.1	–	18.6
HMOR_9.8	Zeolyst	9.8	–	19.5
HMOR_9.5	Zeolyst	9.5	–	19.9
HMOR_6.0	Zeolyst	6.0	<0.002	21.0
HMOR_46	Zeolyst	46	–	–
NaMOR_0.17	Zeolyst	9.1	0.17	–
NaMOR_0.27	Zeolyst	9.0	0.27	–
NaMOR_0.41	Zeolyst	8.7	0.41	–
NaMOR_0.55	Zeolyst	9.0	0.55	6.6
NaMOR_0.90	Zeolyst	9.9	0.90	∼1
HMOR-Ox_15.3	Zeolyst	15.3	–	–
HMOR-Ox_14.2	Zeolyst	14.2	–	–
HMOR-Ox_16.5	Zeolyst	16.5	–	–
HFER_34.5	Zeolyst	34.5	–	3.5
HMFI_12.2	AlSi-Penta	12.2	–	15.4

Praxair) for 3 h at 773 K (0.0167 K s^{-1}) to remove residual organics and to convert NH_4^+ cations to H^+.

^{27}Al magic-angle spinning (MAS) NMR spectra were measured with a Bruker AV-500 spectrometer using a 4-mm MAS broadband probe. The spectra were referenced to octahedral Al^{3+} cations in 1 M aluminum nitrate solutions. Acid forms of the zeolites were kept for ⩾12 h in a desiccator containing aqueous 1 M NaCl (∼96% relative humidity), because these hydration protocols sharpen ^{27}Al NMR lines by weakening quadrupole interactions [27]. The amount of extra-framework Al, measured from these ^{27}Al NMR; the Si, Al, and Na contents (Galbraith Laboratories, ICP-OES); and the nomenclature used are reported in Table 1.

2.2. Steady-state catalytic reactions of DME–CO and DME–CO–H_2O mixtures

DME carbonylation rates and selectivities were measured in a packed-bed stainless steel reactor (8.1 mm i.d., 9.5 mm o.d.) held within a three-zone resistively heated furnace (Applied Test Systems, 3210 series). Temperature was measured using an axial multipoint thermocouple contained within a stainless steel thermowell (1.6 mm o.d.). Catalyst samples (0.2–0.6 g, 125–250 μm particle diameter) were treated in flowing dry air (∼1.67 cm^3 s^{-1} g^{-1}, zero grade, Praxair) for 2 h at 773 K at a heating rate of 0.167 K s^{-1} before cooling in flowing He (∼3.33 cm^3 s^{-1} g^{-1}, UHP, Praxair) to reaction temperatures (420–513 K) and introducing DME (99.5%, Praxair), 95% CO/Ar (UHP, Praxair), or 2% DME/5% Ar/93% CO (99.5% DME, UHP Ar/CO, Praxair) reactant mixtures. The reactant mixtures were dried before use by passing through a CaH$_2$ (0.5 g, 99.99%, Aldrich) bed held at ambient temperature. Water was introduced into the reactant mixture after the CaH$_2$ bed using a syringe pump (Cole-Parmer, model 100 series) in experiments designed to explore kinetic inhibition of carbonylation reactions by water. The reactor effluent was brought via transfer lines held at 423–473 K into a mass spectrometer (MKS Spectra Minilab) or into a gas chromatograph (Agilent

6890) equipped with a methyl-siloxane column (HP-1, 50 m × 0.32 mm × 1.05 µm) connected to a flame ionization detector and a Porapak Q column (80–100 mesh, 12 ft. × 1/8 in.) connected to a thermal conductivity detector. These apparatus and treatment protocols were also used for the studies described in Sections 2.3–2.5.

2.3. Transient reaction studies involving DME–CO and CO cycling

Samples were sequentially contacted with DME–CO reactants and pure CO streams in transient studies designed to probe the nature of carbonylation reactive intermediates and elementary steps. Catalysts were treated in flowing dry air and contacted first with DME–CO mixtures (930 kPa CO, 20 kPa DME, 50 kPa Ar, 438 K) (as described in Section 2.2) for ~5 h to obtain steady-state rates; the system was then brought to ambient pressure and treated in He (3.33 cm^{-1} s^{-1} g^{-1}, UHP, Praxair) until DME levels in the effluent (measured by mass spectrometry) were below 0.02%. The system pressure was then increased to 1 MPa in He before the samples were exposed to either a 95% CO/Ar (UHP, Praxair) or pure CO (99.99%, Praxair) flow at 1 MPa and 438 K for various time intervals, after which DME–CO mixtures were reintroduced at 1 MPa total pressure (930 kPa CO, 20 kPa DME) and 438 K. The transient evolution of methyl acetate (43 amu) and DME (43 and 45 amu) was measured by on-line mass spectrometry with a time resolution of 10 s during these experiments.

2.4. Acetic anhydride reactions with Brønsted acid sites

HMOR_9.8 samples (~0.5 g) treated in dry flowing air (as described in Section 2.2) were exposed to flowing He (3.33 cm^3 s^{-1} g^{-1}, UHP, Praxair) saturated with acetic anhydride (99%, EMD Chemicals; 273 K, 0.11 kPa) and held at 438 K for ~3.5 h. The reactor effluent was analyzed by gas chromatography and mass spectrometry (as described in Section 2.2) to determine the identity and the number of molecules evolved in reactions of acetic anhydride molecules with zeolitic protons. After contact with acetic anhydride, samples were exposed to flowing He (3.33 cm^3 s^{-1} g^{-1}) for ~2 h at 438 K to remove physisorbed molecules before introducing DME/CO/Ar mixtures (3.33 cm^3 s^{-1} g^{-1}; 2/93/5 kPa; 438 K) and monitoring the products formed by mass spectrometry and gas chromatography.

2.5. Isotopic exchange and kinetic isotope effects

Isotopic-exchange experiments were carried out in a gradientless recirculating batch reactor (590 cm^3) as described previously [28]. The reactant stream was circulated (~3.33 cm^3 s^{-1}) over the catalyst bed (~0.5 g; 125–250 µm particle diameter) using a graphite gear micropump (Micropump, model 182–000). Gas samples (1 cm^3) were extracted from the circulating gas stream and analyzed by gas chromatography (Agilent 6890; HP-1 methyl siloxane capillary column; 50 m × 0.32 mm

× 1.05 µm) using mass spectrometry (Agilent 5973) and flame ionization detection. ^{12}C and ^{13}C isotopomer distributions in DME and methyl acetate were measured from ion yields (DME: 46, 47, and 48 amu; methyl acetate: 43, 44, 45, 74, 75, and 76 amu) using deconvolution methods and mass fragmentation patterns for unlabeled molecules [29]. Samples were treated in flowing dry air (3.33 cm^3 s^{-1} g^{-1}, zero grade, Praxair) at 773 K (0.0167 K s^{-1}) for 2 h and then cooled to reaction temperatures before introducing reactants.

^{12}CH$_3$O^{12}CH$_3$ (99.5%, Praxair) and He (UHP, Praxair) mixtures were recirculated over the catalysts held at 438 K for 1 h, followed by evacuation and He purge for ~3.25 h before the samples were exposed to isotopic mixtures to eliminate induction periods. A mixture of ^{12}CH$_3$O^{12}CH$_3$ (99.5%, Praxair) and ^{13}CH$_3$O^{13}CH$_3$ (99 at% ^{13}C, Isotec) isotopomers was contacted with ^{12}CO (UHP, Praxair) on HMOR_9.8 to probe the reversibility of C–O cleavage in DME during carbonylation reactions. CH$_3$OCH$_3$ and CD$_3$OCD$_3$ (99 at%, Isotec) were reacted with CO either separately or as an equimolar mixture to probe the reversibility of C–H bond dissociation steps and the involvement of C–H bonds in kinetically relevant steps during DME carbonylation.

2.6. IR spectroscopic studies of DME, acetic anhydride, and carbon monoxide adsorption

IR spectra were measured with 2 cm^{-1} resolution on self-supporting wafers (~20–40 mg) held within a quartz vacuum cell with NaCl windows using a Nicolet NEXUS 670 IR spectrometer equipped with a Hg–Cd–Te (MCT) detector in the 4000–400 cm^{-1} frequency region. Samples were treated in flowing dry air (~1.67 cm^3 s^{-1}, zero grade, Praxair) at 723 K for 1 h, evacuated at 723 K for 2 h using a diffusion pump (<0.01 Pa dynamic vacuum; Edwards E02) and cooled to 438 K in vacuum before samples were contacted with DME (99.5%, Praxair) or acetic anhydride (99%, EMD Chemicals) for 0.25 h. Samples were treated similarly before cooling to 123 K (using a constant flow of liquid N$_2$) and exposing them to CO (UHP, Praxair) at 123 K. IR spectra were collected for 120 s after each CO dose without intervening evacuation.

2.7. CO adsorption and temperature-programmed desorption studies

Samples (0.3–0.7 g, 125–250 µm pellet diameter) were treated in flowing dry air (~6.67 cm^3 s^{-1} g^{-1}, zero grade, Praxair) at 773 K for 1 h before cooling (at 0.167 K s^{-1}) to 253 K using liquid nitrogen. A mixture of 1% CO/He (UHP, Praxair; ~1.67 cm^3 s^{-1} g^{-1}) was introduced for 0.5–0.75 h on samples held at 253 K before flushing CO(g) with flowing He (~1.67 cm^3 s^{-1} g^{-1}, UHP, Praxair) for 1.5 h to remove weakly adsorbed CO. The temperature was then increased to 523 K (0.167 K s^{-1}) and held at 523 K for 360 s. The concentration of CO (28 amu) in the He stream was monitored continuously by mass spectrometry (MKS Orion Compact).

2.8. UV–visible spectroscopy of Co-exchanged zeolites

Co-exchanged HMOR_9.8 and HMFI_12.2 catalysts were prepared by contacting zeolites with 0.1 M $Co(NO_3)_2 \cdot 6H_2O$ solutions (Sigma Aldrich, CAS 10026-22-9, 98+%) for 24 h at 353 K. Samples were filtered, washed with 0.5 L of deionized water, dried in ambient air overnight, and treated in flowing dry air (zero grade, Praxair) at 773 K (0.0167 K s^{-1}) for 3 h. The resulting Co/Al ratios measured by elemental analysis (Galbraith Laboratories, ICP-OES) were 0.32 for MOR_9.8 and 0.16 for MFI_12.2.

UV–vis spectra were measured using a Cary 400 Bio spectrophotometer (Varian) and an in situ flow cell (Harrick) with a diffuse reflectance accessory. MgO powders treated in He at 300 K (Praxair, UHP, dried on a 13X molecular sieve) were used as reference. Reflectance (R) data were converted to pseudo-absorbance [$F(R)$] using the Schuster–Kubelka–Munk formalism. Cobalt-exchanged zeolite samples were treated in He flow by heating to 373 K (0.083 K s^{-1} and hold for 1 h), then to 523 K (0.083 K s^{-1} and hold for 1 h), and finally to 773 K (0.083 K s^{-1} and hold for 1 h). Samples were then cooled to ambient temperatures (~303 K), and the spectra were measured in He flow. Linear combination methods and peak positions and relative absorption coefficients reported previously [30–32] were used to measure the relative distribution of Co cations among α, β, and γ sites in HMOR_9.8 and HMFI_12.2. This method provides a semiquantitative measure of Al pair site occupation in zeolites, because the siting of Co cations depends on the method of Co incorporation, the dehydration procedure, the presence of co-cations, and the total Co concentration [30–32].

3. Results and discussion

3.1. Steady-state DME carbonylation rates, kinetics, and mechanism

Fig. 1 shows methyl acetate and methanol formation rates on HMOR_9.8 at 438 K as a function of reaction time after treating samples in flowing dry air at 773 K before exposure to DME–CO reactants (930 kPa CO, 20 kPa DME). Steady-state carbonylation rates and methyl acetate selectivities (>99%) were achieved after ~4 h. Methyl acetate synthesis rates increased initially with reaction time, whereas methanol synthesis rates decreased concurrently during this induction period (Fig. 1). This induction period was not observed when samples were exposed to DME pulses ($DME_{dosed}/Al = 1$) at 438 K and then flushed with He for 2 h before contact with DME–CO reactants.

DME reacted with acidic protons in H-MOR and HMFI_12.2 ($DME_{dosed}/Al \leqslant 1$) to form methyl groups and water; the DME/Al uptake stoichiometry was 0.5 ± 0.05 and 0.51 on these samples [24]. DME molecules first react with an acidic proton to form a methanol molecule and a methyl group; the methanol thus formed can then react with another Brønsted acid site to form $H_2O(g)$ and a second methyl group [24]. During steady-state DME–CO reactions, some CH_3OH molecules leave the reactor before they react with another proton, because of competing reactions of DME reactants with such protons.
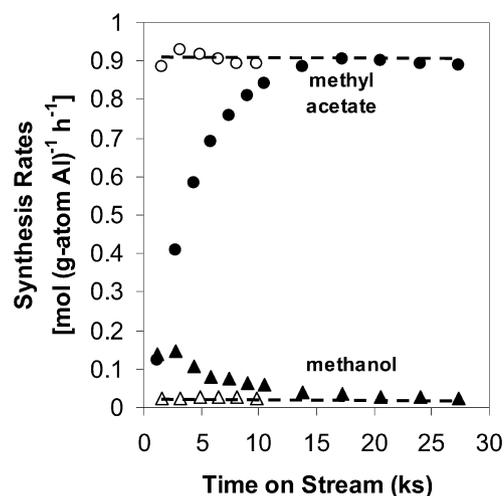

Fig. 1. Methyl acetate (●,○) and methanol (▲,△) synthesis rates without DME pretreatment (solid symbols) and with DME pretreatment ($DME_{dosed}/Al = 1$, 7.2 ks He purge, 438 K, open symbols) [HMOR_9.8, 930 kPa CO, 20 kPa DME, 438 K].
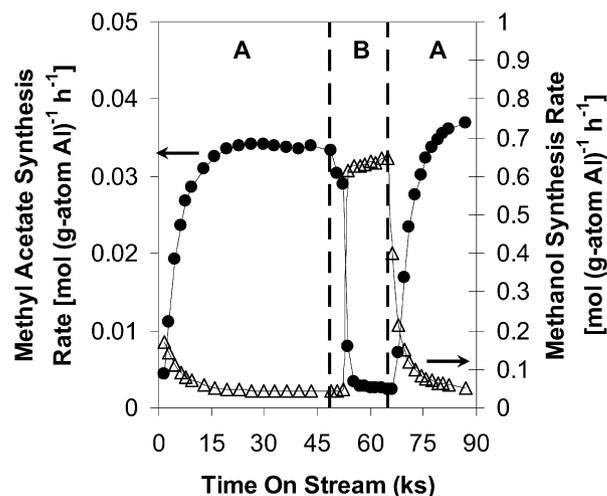

Fig. 2. Methyl acetate (●) and methanol (△) synthesis rates in (A) DME–CO mixtures (26 kPa DME, 123 kPa CO) and in (B) DME–CO–H_2O mixtures (26 kPa DME, 123 kPa CO, and 1.1 kPa H_2O) [HMOR_9.8, 423 K].

The low methanol selectivities (<1%) measured at steady state indicate that essentially anhydrous conditions prevail during steady-state DME carbonylation. Induction periods disappeared when catalysts are exposed to DME before reaction, because exchange sites become saturated with methyl groups and the water formed is removed from the catalyst bed before catalysis.

Water formed during saturation of exchange sites with CH_3 groups inhibits carbonylation rates. Fig. 2 shows that water (1.1 kPa) added to DME–CO reactants (26 kPa DME, 123 kPa CO, 423 K, HMOR_9.8) decreased methyl acetate formation rates from 0.034 to 0.0024 mol (g-atom Al)$^{-1}$ h^{-1} and increased methanol formation rates by a factor of 14; no acetic acid or other products were detected with or without added water. Methanol and methyl acetate synthesis rates returned gradually (~4 h) to their initial values after the added H_2O was removed. This reactivation period resembled those observed during initial exposure to DME–CO reactants.
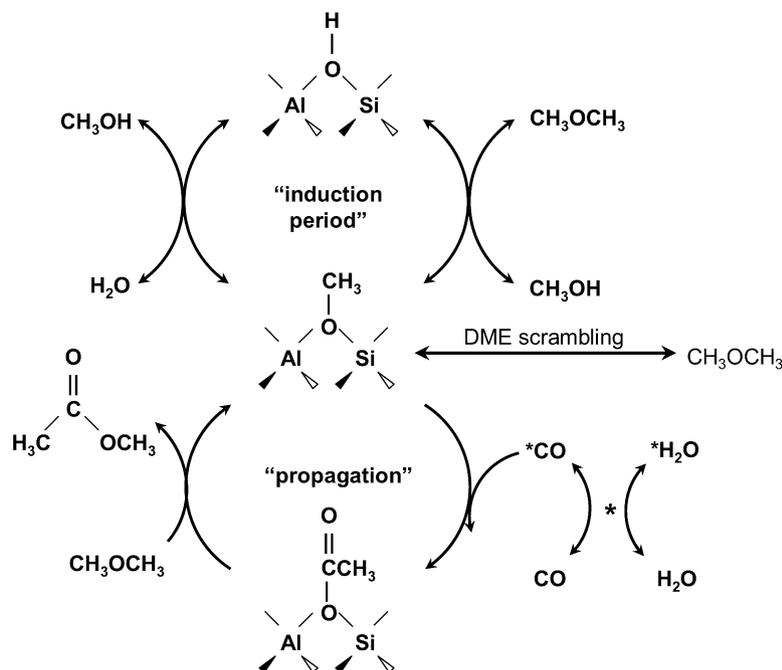
Scheme 1. Proposed elementary steps for carbonylation of dimethyl ether on acidic zeolites.

Methyl acetate synthesis rates were proportional to CO pressure (0–930 kPa) and independent of DME pressure (0.8–66.8 kPa), both under anhydrous conditions and when H_2O (0.5 kPa) was added [24]. Thus, active sites remained saturated with CH_3 groups even in the presence of H_2O, because methyl acetate synthesis rates remained independent of DME pressure at H_2O levels that strongly inhibit carbonylation rates. The first-order dependence on CO (up to ∼1 MPa) and the zero-order kinetics in DME require non-competitive binding of DME and CO or Eley–Rideal-type reactions involving gas-phase CO species with bound DME-derived intermediates at saturation coverage. Hence, water may inhibit reaction rates either by adsorbing competitively with CO or by decreasing the reactivity of surface methyl groups toward CO molecules. The linear dependence of carbonylation rates on CO reflects the very low occupancy of any CO binding sites prevalent during catalysis; thus, the presence or involvement of chemisorbed CO species cannot be confirmed by in situ spectroscopic methods. As a result, the identity of CO-binding centers remains unclear at this time, but our experimental observations are consistent with the sequence of elementary steps detailed below (and shown in Scheme 1). In what follows, we provide evidence for this mechanistic proposal and discuss, in this context, possible carbonylation sites.

1. Quasi-equilibrated adsorption of CO on a binding site (^{*a}):

$$CO + {}^{*a} \underset{}{\overset{K_1}{\rightleftharpoons}} {}^{*a}CO.$$
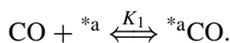
2. Quasi-equilibrated (competitive) H_2O adsorption onto this CO binding site:

$$H_2O + {}^{*a} \underset{}{\overset{K_2}{\rightleftharpoons}} {}^{*a}H_2O.$$
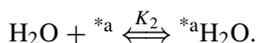
3. Quasi-equilibrated reaction of DME with acidic protons to form methanol and a chemisorbed methyl group at zeolite-exchange sites:

$$CH_3OCH_3 + {}^{*b}H \underset{}{\overset{K_3}{\rightleftharpoons}} CH_3OH + {}^{*b}CH_3.$$

4. Quasi-equilibrated reaction of methanol with acidic protons to form water and a second chemisorbed methyl group at zeolite-exchange sites:

$$CH_3OH + {}^{*b}H \underset{}{\overset{K_4}{\rightleftharpoons}} H_2O + {}^{*b}CH_3.$$
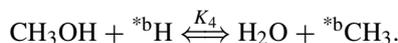
5. Irreversible reaction of activated CO with a methyl group to form an acetyl group at zeolite-exchange sites:

$${}^{*a}CO + {}^{*b}CH_3 \overset{k_5}{\longrightarrow} {}^{*b}COCH_3 + {}^{*a}.$$
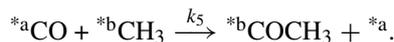
6. Reaction of DME with an acetyl group to form methyl acetate and to re-form a methyl group at zeolite-exchange sites:

$$CH_3OCH_3 + {}^{*b}COCH_3 \overset{k_6}{\longrightarrow} CH_3COOCH_3 + {}^{*b}CH_3.$$
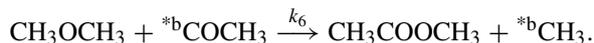
7. Quasi-equilibrated CH_3 exchange between DME and surface CH_3 groups:

$$\mathbf{CH_3OCH_3} + {}^{*b}CH_3 \underset{}{\overset{K_7}{\rightleftharpoons}} {}^{*b}CH_3 + CH_3OCH_3.$$
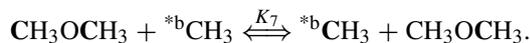
Two distinct catalytic sites are involved in these pathways: zeolite-exchange sites (^{*b}) that stabilize acidic protons and methyl and acetyl groups, and CO-binding centers (^{*a}) that non-competitively bind DME and CO. The quasi-equilibrium assumption for CO, H_2O, and DME adsorption, and the pseudo-steady-state approximation for all reactive intermediates gave a rate equation for methyl acetate synthesis [Eq. (1); derivation in

Appendix A] of the form

$$r_{CH_3COOCH_3} = \frac{K_1 k_5 P_{CO} C_{T,a}}{1 + K_1 P_{CO} + K_2 P_{H_2O}}$$
$$\times \left(\frac{1}{1 + \frac{P_{H_2O}}{K_4 P_{CH_3OH}} + \frac{K_1 k_5 P_{CO} C_{T,a}}{k_6 P_{DME}(1 + K_1 P_{CO} + K_2 P_{H_2O})}} \right), \quad (1)$$

in which turnover rates (per H^+) are not normalized by the concentration of CO binding sites, $C_{T,a}$, because of their uncertain identity.

In these elementary steps, induction periods reflect the initial slow replacement of protons with methyl groups via reactions with DME. These steps initiate a propagation cycle that ultimately avoids H_2O formation by re-forming CH_3 groups via methoxylation of acetyl intermediates. When CH_3 groups are the most abundant reactive intermediates (MARI) and the concentration of surface-bound CO is low [or reactions occur directly with unbound CO(g)], these steps lead to a carbonylation rate equation consistent with rate data. Methyl acetate synthesis rates depend only on CO pressure and on the number of CO binding sites ($C_{T,a}$), or CH_3 binding sites if reaction occurs with CO(g), in step 5 [Eq. (2)]:

$$r_{CH_3COOCH_3} = K_1 k_5 P_{CO} C_{T,a}. \quad (2)$$

If CO(g) reacted directly with MARI CH_3 groups to form acetyl groups, then methyl acetate synthesis rates [Eq. (3), per H^+] would show a kinetic dependence identical to that for reactions with any CO bound present at low fractional coverages [Eq. (2)]:

$$r_{CH_3COOCH_3} = \frac{k_5 P_{CO}}{1 + \frac{P_{H_2O}}{K_4 P_{CH_3OH}} + \frac{k_5 P_{CO}}{k_6 P_{DME}}} \approx k_5 P_{CO}. \quad (3)$$

If CO(g) reacted directly, then H_2O could inhibit rates either by decreasing the rate of CO with CH_3 or by altering the concentration or reactivity of the latter. If CH_3 concentrations were influenced, however, H_2O would adsorb competitively with DME-derived intermediates and carbonylation rates would become dependent on DME pressure as protons become the MARI at high H_2O concentrations. In such instances, Eq. (3) would become sensitive to both H_2O and DME [Eq. (4)], in contradiction to the experimental evidence provided herein:

$$r_{CH_3COOCH_3} = \frac{K_3^{1/2} K_4^{1/2} k_5 P_{DME}^{1/2} P_{CO}}{P_{H_2O}^{1/2}}. \quad (4)$$

Carbonylation rates remained independent of DME pressure even when H_2O was added and markedly inhibited such rates [24]; thus, H_2O does not inhibit rates by replacing CH_3 groups with H^+, and H_2O inhibition must reflect either a decrease in CH_3 reactivity in carbonylation reactions or the competitive binding of CO and H_2O on sites that bind reactive CO species. Below we provide spectroscopic and isotopic evidence to confirm the identity of proposed surface intermediates and of elementary steps in Scheme 1 (steps 5–7).

3.2. In situ IR spectroscopic studies of DME reactions

IR spectra were collected after a sequence of DME pulses (DME/Al = 1.2 cumulative total) on HMOR_9.8 held within a closed system (Fig. 3). The intensity of acidic O–H stretches (3610 cm^{-1}, Fig. 3a) decreased sharply with the number of DME pulses, whereas bands for C–H stretches concurrently became more intense (Fig. 3b). Evacuation (<0.01 Pa) after dosing DME (DME/Al = 1.2) restored some of the initial O–H band intensity (∼20%, Figs. 3c and 3d) but did not influence the strong band at 2978 cm^{-1} or the weaker bands at 2868 cm^{-1} and 2855 cm^{-1}, even after 1 h at 438 K. The bands at 2978 and 2868 cm^{-1} correspond to antisymmetric and symmetric C–H stretches in methyl groups, respectively. Such bands were detected also after exposing H-MFI to DME or methanol at 473–523 K [33,34]. The weak band at 2855 cm^{-1} was assigned to methyl groups at silanols present at external H-MFI surfaces (SiOCH$_3$) [33]. The bands and shoulders at 3011, 2971, 2947, and 2844 cm^{-1} were previously assigned to DME molecules hydrogen-bonded to acidic O–H groups [33]; these bands disappeared on evacuation at 438 K for ∼0.4 h. CH_3 groups and hydrogen-bonded DME coexist during contact with DME, because any H_2O formed (in steps 3 and 4) remains within the closed system until evacuation and can displace CH_3 (the reverse of step 4) during evacuation to re-form some OH groups. Molecular simulations have confirmed the persistent nature of CH_3 groups in HZSM-5 during methanol-to-olefin (MTO) reactions [35], and ^{13}C MAS NMR has detected them after contacting methanol with H-Y, HZSM-5, H-SAPO-34, and H-ZSM-11 at 423–473 K [36–38]. These IR studies, taken together with the DME$_{adsorbed}$/Al adsorption stoichiometry of ∼0.5 on HMOR_6.0, HMOR_9.8, and HMFI_12.2 [24], provide spectroscopic and stoichiometric evidence for the prevalence and relevance of CH_3 groups at Brønsted acid sites during DME carbonylation reactions.

3.3. Isotopic evidence for the identity, kinetic relevance, and reversibility of carbonylation elementary steps

Experimental protocols for ^{12}C–^{13}C mixed isotope studies initially involved exposing the HMOR_9.8 sample to ^{12}CH$_3$O^{12}CH$_3$–He mixtures (Section 2.5), to avoid reactions of methyl groups with any H_2O formed and retained during the induction period. These reactions would form methanol [36] and lead to isotopic scrambling via elementary steps unavailable during anhydrous DME carbonylation at the steady state. These DME pretreatment protocols also eliminate induction periods, required to form methyl groups, so that steady-state carbonylation occurs immediately on contact with ^{12}CH$_3$O^{12}CH$_3$–^{13}CH$_3$O^{13}CH$_3$–^{12}CO mixtures and exclusively via the relevant propagation steps 5 and 6 in Scheme 1.

Figs. 4a and 4b show the concentrations of DME and methyl acetate isotopomers with increasing reaction time. Methyl groups scramble to form ^{12}CH$_3$O^{13}CH$_3$ more than 70 times faster than they convert to methyl acetate; consistent with this, isotopomers reached their binomial distribution at reaction times leading to only ∼1% DME conversion to methyl acetate
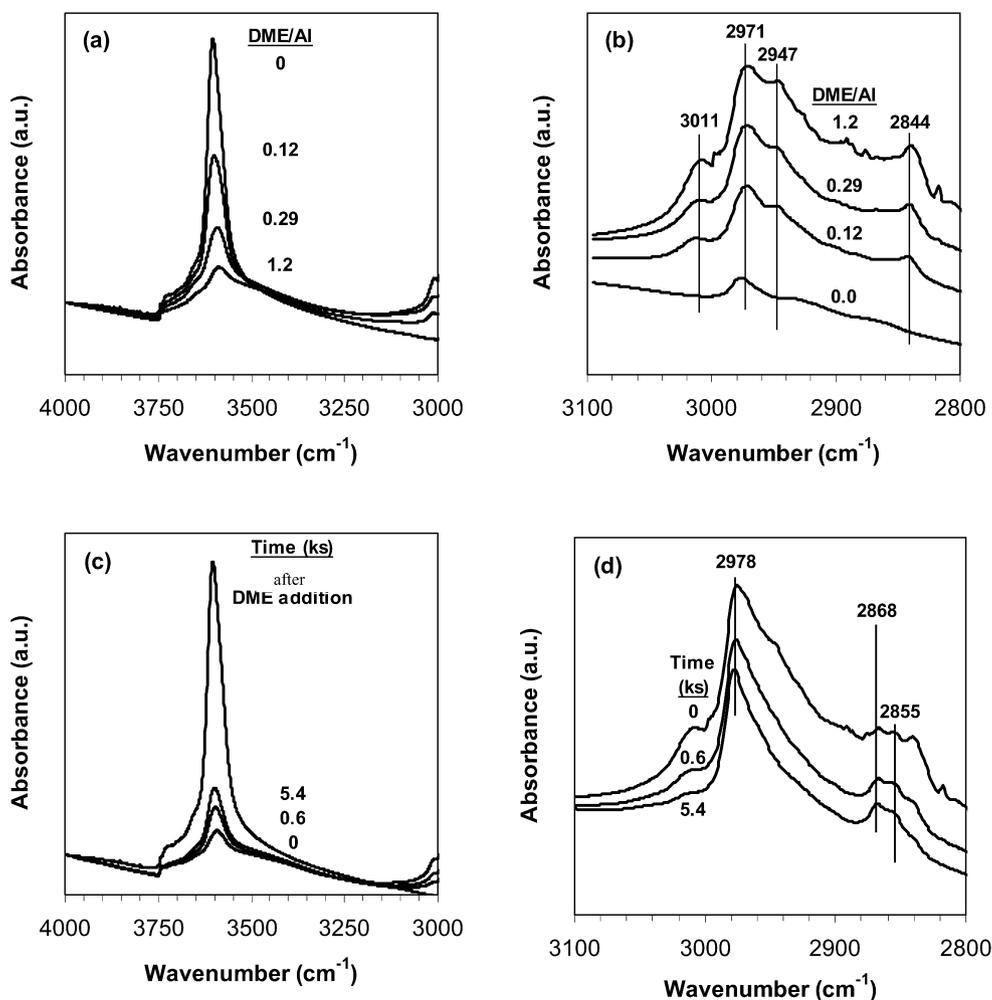
Fig. 3. Infrared spectra of HMOR_9.8 at 438 K (treated at 723 K in air within the infrared cell and cooled to 438 K in vacuum) of (a) O–H and (b) C–H stretching regions during exposure to DME (DME/Al = 0–1.2) and (c) O–H and (d) C–H stretching regions following exposure to DME (DME/Al = 1.2) and evacuation for 0–5.4 ks.
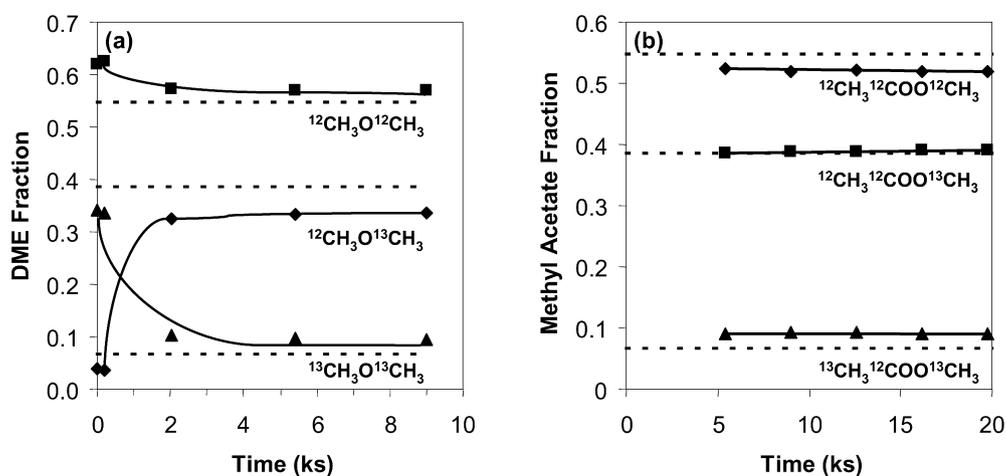

Fig. 4. Mole fraction of (a) DME and (b) methyl acetate isotopomers (solid symbols) and calculated binomial isotopomer distributions (dotted lines) during reactions of $^{12}CH_3O^{12}CH_3$, $^{13}CH_3O^{13}CH_3$, and ^{12}CO following pretreatment at 438 K in 4 kPa $^{12}CH_3O^{12}CH_3$ for 1 h [2.35 kPa $^{12}CH_3O^{12}CH_3$, 2.03 kPa $^{13}CH_3O^{13}CH_3$, 97.4 kPa ^{12}CO, 0.5 g HMOR_9.8, 438 K].

(~2 ks). Rapid CH_3 scrambling reflects rapid methoxylation of surface methyl groups by DME (step 7) or fast reversible formation of trimethyloxonium ions; the latter were suggested

by theoretical calculations on chabazite [39] and may provide a source of methyl groups for CO insertion steps, as for alkylation in superacids [40] and methanol homologation on ZSM-5 [35].

These data also suggest that methoxylation of acetyls (step 6) may be fast and kinetically inconsequential. However, fast methyl scrambling prevents us from determining whether CO insertion occurs before or after its dissociation from methyl acetate isotopomers. No ^{13}C (<1% detection limit) was detected in CO(g) or in the carbonyl group of methyl acetate (from COCH$_3$ mass fragments) during reactions of $^{12}CH_3O^{12}CH_3$–$^{13}CH_3O^{13}CH_3$–^{12}CO mixtures, indicating that carbonyl groups in methyl acetate are derived only from $^{12}CO(g)$.

Kinetic isotope effects from methyl acetate synthesis rates with CH$_3$OCH$_3$–CO and CD$_3$OCD$_3$–CO mixtures were very small ($k_H/k_D = 1.06$) at 438 K on HMOR_9.8, suggesting that C–H bonds are not cleaved or formed in kinetically relevant steps. In addition, H-D scrambling in DME or methyl acetate did not occur during reactions of CH$_3$OCH$_3$–CD$_3$OCD$_3$–CO mixtures at 438 K, except to form CH$_3$OCD$_3$ as a result of fast methyl scrambling.

3.4. Transient reactions of DME–CO and CO cycling

CO reactions with surface methyl groups to form acetyl species were proposed as the sole kinetically relevant step in DME carbonylation to methyl acetate on HMOR_9.8 [24]. The abrupt replacement of DME–CO mixtures with pure CO for various time intervals led to the formation of precursors to methyl acetate; however, these precursors desorbed only after pure DME or DME–CO reactants were reintroduced. Subtracting steady-state rates from "excess" methyl acetate formation rates and integrating over time during contact with DME–CO reactants led to an estimate of the number of methyl acetate precursors formed (per Al) during previous exposure of preformed methyl groups to CO(g). These reflect, in turn, the number of stranded acetyls formed, which increased monotonically with increasing time of exposure to CO(g) (Fig. 5). Acetyls desorb rapidly (as methyl acetate) on contact with DME or DME–CO mixtures via reactions with DME (step 6), in a step that

Table 2
Initial carbonylation rate calculated from transient reactions of methyl groups with CO and steady-state methyl acetate synthesis rates [transient: 1000 kPa CO, 438 K; steady-state: 20 kPa DME, 930 kPa CO, 438 K]

Zeolite	Initial carbonylation rate [mol (g-atom Al)$^{-1}$ h^{-1}]	Steady-state methyl acetate synthesis rate [mol (g-atom Al)$^{-1}$ h^{-1}]
HMOR_9.8	0.42[*]	0.82
HMOR_8.9	0.19	0.55
HMOR_16.5	0.14	0.32
HMFI_12.2	Not detected	0.027

[*] 950 kPa CO.

restores the methyl groups consumed to form acetyl intermediates, completing the catalytic cycle. The replacement of DME–CO mixtures with pure CO led to an immediate decrease in methyl acetate synthesis rates to undetectable values, indicating that any acetyls present during catalysis desorbed only after methoxylation by DME. The replacement of DME–He (instead of DME–CO) mixtures with pure CO before re-exposure to DME–He at 438 K gave undetectable rates [<0.01 mol (g-atom Al)$^{-1}$ h^{-1}] after a spike in methyl acetate formation on re-exposure of samples to DME/He mixtures; the absence of CO in the gas phase precludes the continuing replacement of the acetyls used to form methyl acetate during this initial contact, and rates become undetectable as acetyls are depleted (step 6).

The initial rate of CO–CH$_3$ reactions can be measured from the number of excess methyl acetate molecules formed (per Al) during transient experiments by determining the initial slope of excess methyl acetate concentrations as a function of CO exposure time (Table 2). These rates reflect the dynamics of CO reactions on a surface initially saturated with methyl groups, which reflects, in view of the measured steady-state kinetic dependence, surface and kinetically relevant steps during carbonylation catalysis. Reaction rates decrease with CO exposure time, as methyl groups are depleted in reactions forming CH$_3$CO species. Fig. 5 shows that CO reactions with CH$_3$ groups are faster on HMOR_9.8 than on HMOR_8.9, HMOR-Ox_16.5, or HMFI_12.2, as is also found in the case of steady-state carbonylation, indicating that HMOR_9.8 is a superior catalyst because it carbonylates methyl groups more efficiently than the other samples.

The rates (per Al) of CO reactions with CH$_3$ groups are ~2 times lower than for steady-state DME carbonylation (Table 2) except for HMFI_12.2, on which we could not detect excess methyl acetate after exposure to CO. These differences between steady-state and transient carbonylation rates may reflect nonuniform reactivity of methyl species, depending on their location within channels or on their position relative to other CH$_3$ or CH$_3$CO groups, or the carbonylation of trimethyloxonium ions during steady-state catalysis instead of methyl groups during these transient experiments. The striking parallel between transient and steady-state rates led us to conclude, however, that CH$_3$CO formation via CO reactions with surface CH$_3$ is indeed the kinetically relevant elementary step in DME carbonylation on all samples, as was also indicated by the measured dependence of steady-state rates on DME and


Fig. 5. Excess methyl acetate formed per Al during reaction with DME–CO mixtures [930 kPa CO, 20 kPa DME, 50 kPa Ar, 438 K] immediately following exposure to pure CO [1000 kPa CO (950 kPa CO for HMOR_9.8)] for varying flush times at 438 K on HMOR_9.8 (◆, A), HMOR_8.9 (▲, B), HMOR-Ox_16.5 (■, C), and HMFI_12.2 (●, D); values determined by first- (—) and second-order (- - -) rate dependences on methyl group concentration.
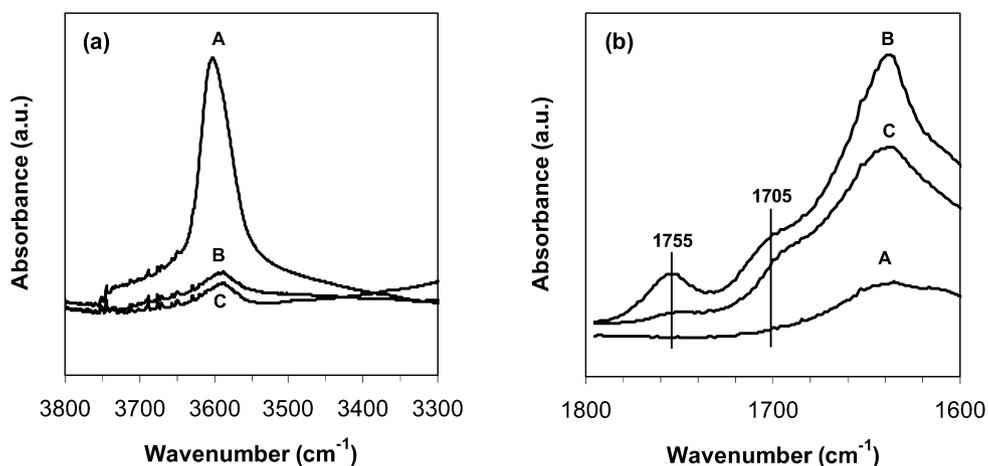
Fig. 6. Infrared spectra of the (a) O–H and (b) C=O regions following pretreatment in air at 773 K for 1 h and cooling to 438 K (A), acetic anhydride addition followed by evacuation (B), and following DME addition (DME/Al > 1) to acetic anhydride-treated samples for 7.2 ks and evacuation (C) [HMOR_9.8, 438 K].

CO pressures. The differences in catalytic carbonylation rates among the various HMOR samples do not reflect differences in the number of available CH_3 groups, because samples with similar Al content (HMOR_9.8 and HMOR_8.9) and CH_3/Al stoichiometries gave different steady-state carbonylation rates. These differences may also reflect a range in reactivity of CH_3 groups (for reactions with CO) depending on their location (in pockets or channels in MOR) or on the number and proximity of Al centers, CH_3 groups, or acetyls; differences in the retention of water among zeolite structures may also contribute to these reactivity trends, in light of the strong kinetic inhibition by water.

3.5. Formation of surface acetyls and their reaction with dimethyl ether

We have proposed that acetyl groups formed by dissociative adsorption of acetic anhydride (or by carbonylation of CH_3 groups) react with DME to form methyl acetate molecules (step 6, Scheme 1). We find, in accordance with previous studies [41], that acetic anhydride reacts below 400 K with O–H groups in H-MFI to form CH_3CO groups. The IR band for acidic OH groups (3610 cm^{-1}) in HMOR_9.8 (Fig. 6a) weakened on exposure to acetic anhydride (dose: 1.5 per Al) at 438 K for 0.25 h; two bands appeared at 1705 and 1755 cm^{-1} (Fig. 6b), assigned to C=O stretches in acetyls (CH_3CO) [41]. But this O–H band did not disappear on exposure to acetic anhydride, because it cannot access Brønsted acid sites within side pockets in MOR. The O–H and acetyl bands were unchanged during subsequent evacuation, but disappeared on contact with DME at 438 K (Fig. 6b). DME reacts with these CH_3CO groups to form methyl acetate and surface methyl groups; the latter were evident from their C–H stretches at 2978 and 2868 cm^{-1} (not shown).

HMOR_9.8 exposed to acetic anhydride (0.11 kPa) at 438 K (Section 2.4) led to methyl acetate synthesis rates temporarily higher than steady-state rates (Fig. 7) on subsequent contact with DME/CO/Ar mixtures (2/93/5 kPa; 438 K; 3.33 cm^3 g^{-1} s^{-1}), as a result of fast methoxylation of previ-
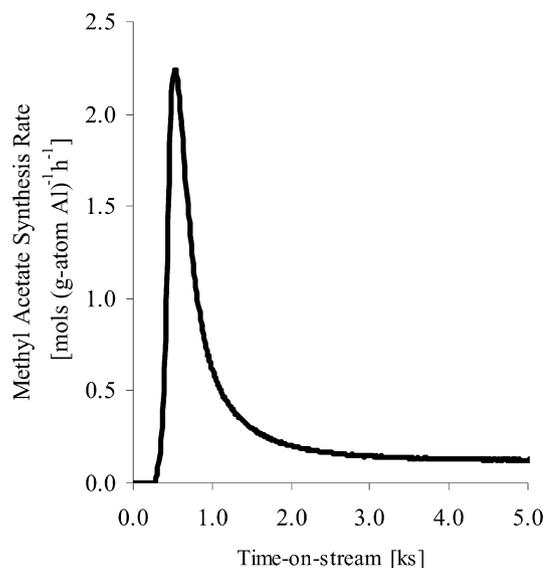

Fig. 7. The rate of methyl acetate upon re-introduction of DME–CO reactants (93 kPa CO, 2 kPa DME, 5 kPa Ar, 438 K) on HMOR_9.8 after exposure to acetic anhydride–He (0.11 kPa acetic anhydride, 100 kPa He) at 438 K for ~3.5h.

ously formed acetyls. The concurrent formation of acetic acid or acetic anhydride was not observed. These data provide spectroscopic and stoichiometric evidence for CH_3 and CH_3CO groups at Brønsted acid sites and for the high reactivity of acetyl groups with DME to form methyl acetate and adsorbed methyl species (step 6).

3.6. Assessment of CO binding sites from IR spectra and desorption dynamics of chemisorbed CO

The nature of CO reactions with CH_3 groups and the CO binding sites required remain unclear, but marked differences in carbonylation reactivity among catalysts with similar Si/Al ratio (Fig. 8) appear to reflect kinetic nonuniformity of active sites involved in CO–CH_3 reactions (Section 3.4). Extraframework Al atoms can act as Lewis acid centers that bind CO [42–44], but carbonylation rates did not vary in a systematic
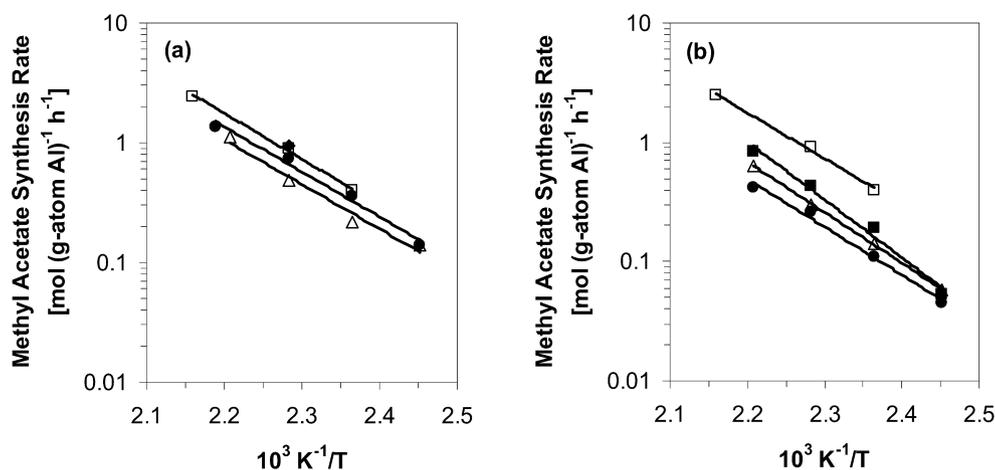
Fig. 8. Arrhenius plot of methyl acetate synthesis rates on (a) H-MOR (Si/Al ∼ 10) from various sources: HMOR_9.5 (◆), HMOR_9.8 (□), HMOR_8.9 (●), HMOR_10.1 (△) and (b) on HMOR_9.8 refluxed in 1.5 M oxalic acid for 3 h (b): no oxalic acid treatment (□), 313 K (■), 343 K (△), and 323 K (●) [930 kPa CO, 20 kPa DME].
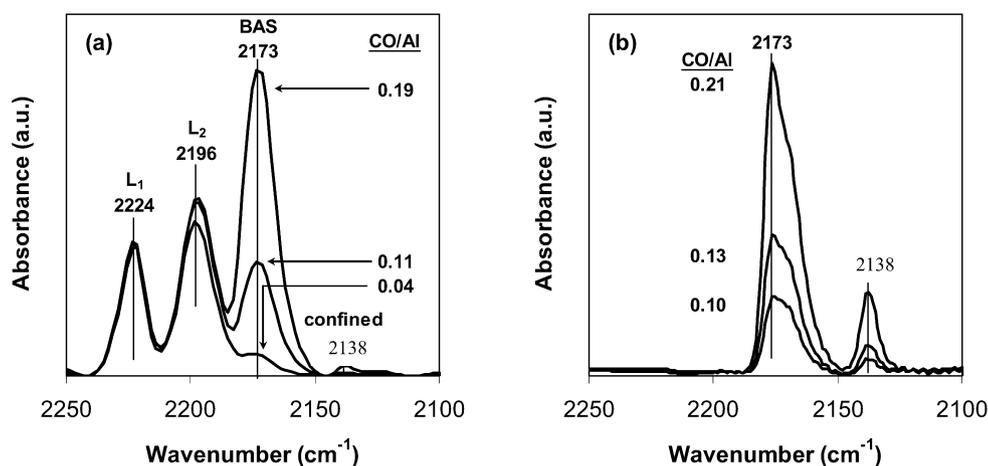

Fig. 9. Infrared spectra of CO doses adsorbed at 123 K on (a) HMOR_9.8 (CO/Al = 0.04–0.19) and (b) HMOR_9.8 (CO/Al = 0.10–0.21) following water pre-adsorption (0.042 H$_2$O/Al) at 298 K and degassing for 0.5 h before cooling to 123 K.

manner with the number of extra-framework Al atoms measured by ^{27}Al MAS NMR (Table 1). Here we examine IR features of CO adsorbed at low temperatures and CO temperature-programmed desorption to explore the nature and number of potential CO binding sites as well as their catalytic consequences.

CO interacted only with Lewis acid centers on HMOR on initial exposure, leading to C=O stretches at 2224 (L$_1$) and 2196 cm^{-1} (L$_2$) (Fig. 9a). The L$_1$ band was assigned to CO on strong Lewis acid sites (e.g., extra-framework Al^{3+}) in H-MOR [44] and SiO$_2$–Al$_2$O$_3$ [45]. L$_2$ sites correspond to penta-coordinated Al^{3+} centers that are more weakly acidic than L$_1$ sites [46]. All Lewis acid centers became saturated before CO interacted with acidic O–H groups via H-bonding ($\nu_{C=O}$ = 2173 cm^{-1}) or with channel walls via van der Waals interactions ($\nu_{C=O}$ = 2137 cm^{-1}). The band at 2173 cm^{-1} strengthened as the band for acidic O–H groups (3610 cm^{-1}) shifted to lower frequencies and broadened (∼3300 cm^{-1}, not shown), consistent with interactions mediated by hydrogen bonding [44,47,48]. Water pre-adsorbed at 298 K (H$_2$O/Al =

0.042) inhibited CO adsorption at 123 K on L$_1$ and L$_2$ sites, but did not influence CO interactions with OH groups (2173 cm^{-1}) or with channel walls (2137 cm^{-1}) (Fig. 9b). The saturation intensities of the L$_1$ and L$_2$ bands are shown in Fig. 10 for HMOR samples with similar Si/Al ratios (∼10). Methyl acetate synthesis rates did not vary monotonically with L$_1$ or L$_2$ intensities (from peak areas normalized by those for Si–O–Si overtones at 2110–1760 cm^{-1}) (Fig. 11a).

The total number of CO binding sites was measured from the amount of CO adsorbed at 253 K and CO pressures leading to saturation of L$_1$ and L$_2$ sites. CO/Al ratios increased from 0.01 in the parent mordenite (HMOR_9.8) to 0.03–0.04 in samples dealuminated by treatment with oxalic acid (Table 3). However, carbonylation rates did not vary in any systematic manner with the measured number of CO binding sites (Fig. 11b), suggesting that strongly bound CO on Lewis acid sites is not involved in carbonylation reactions. Carbonylation rates are proportional to CO pressure (up to >1 MPa), indicating that any CO bound strongly enough to be detectable in spectroscopic studies is unlikely to be involved in kinetically relevant reactions of CO.

3.7. Studies of H-MOR with different Brønsted acid site concentrations

The requirement for Brønsted sites was explored by varying the number of H^+ in H-MOR by changing Na/Al or Si/Al ratios and by chemical dealumination. Methyl acetate synthesis rates (per available H^+) increased monotonically with increasing H^+ concentration (H^+/Al) and proximity (Fig. 12), a finding inconsistent with the sole involvement of H^+ species of uniform reactivity in stabilizing reactive intermediates required for kinetically relevant carbonylation steps. The reactivity of methyl or trimethyloxonium groups at Brønsted acid sites appears to depend on the number and identity of vicinal sites or on the location of such sites in channel or side pockets.

The possibility that proximity among CH_3 groups influences their reactivity was explored by describing the trends in Fig. 5 with rates that depend on (CH_3) or $(CH_3)^2$. Carbonylation rates depend slightly more strongly than linearly on (CH_3), but these trends probably merely indicate that more reactive CH_3 re-

act earlier during stoichiometric carbonylation of previously formed CH_3 groups, perhaps for reasons unrelated to their relative proximity. Although the Al or CH_3 proximity requirements remain unclear at this time, these studies unequivocally show that Brønsted acid sites are required for carbonylation.

3.8. Requirement for CO binding on a separate site for carbonylation of CH_3

The formation of C–C bonds via CO insertion into O–CH_3 bonds in adsorbed methyl groups involves CO-derived species that do not compete with DME-derived CH_3 groups for binding sites. These data do not allow us to discern among three possible mechanistic hypotheses:

(i) Unbound CO(g) reacts directly with surface CH_3 groups.
(ii) CO reacts after binding (non-competitively) on a site already containing a CH_3 group.
(iii) CO reacts after binding on a site vicinal to a CH_3 group (on which CH_3 does not bind).

Proposal (i) seems inconsistent with the effect of zeolites structure and H^+ density (Fig. 12) on turnover rates (per H^+), because all H^+ in all zeolites saturate with CH_3 via reaction with DME. H_2O inhibition effects also cannot be reconciled with this proposal, because surfaces remain saturated with CH_3 groups and carbonylation remains zero-order in DME even in

Fig. 10. Infrared spectra of CO doses adsorbed at 123 K following saturation of 2224 and 2196 cm^{-1} bands with CO on HMOR_9.8 (A), HMOR_8.9 (B), HMOR_9.5 (C), and HMOR_10.1 (D).

Table 3
Concentration of CO bound per Al atom at 253 K from CO temperature-programmed desorption studies

| Zeolite	CO/Al
HMOR_9.8	0.021
HMOR_9.5	0.0092
HMOR_10.1	0.016
HMOR_8.9	0.0033
HMOR-Ox_14.2	0.038
HMOR-Ox_16.5	0.029
HMFI_12.2	0.013
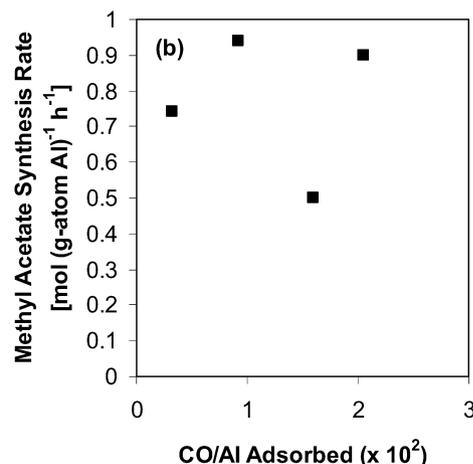
Fig. 11. Methyl acetate synthesis rates per Al atom as functions of (a) saturated CO adsorption infrared band areas of peaks centered at 2224 cm^{-1} (L_1, ▲) and at 2196 cm^{-1} (L_2, ○) (spectra collected at 123 K and normalized per Si–O–Si overtone areas located at 2110–1760 cm^{-1}) and (b) CO/Al adsorption ratios determined by CO temperature-programmed desorption of CO pre-adsorbed at 253 K [20 kPa DME, 930 kPa CO, 438 K].
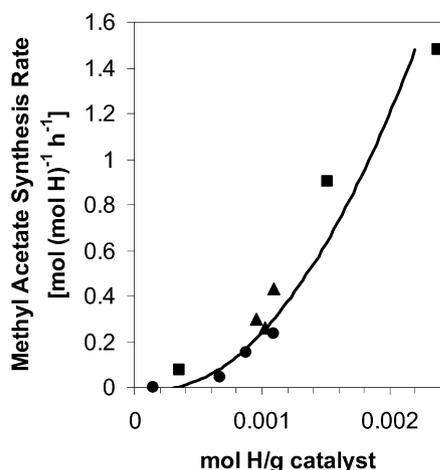
Fig. 12. Methyl acetate synthesis rates per available H^+ on Na-exchanged samples (HMOR_9.8, NaMOR_0.27, NaMOR_0.41, NaMOR_0.55, NaMOR_0.90) (●) on samples with different Si/Al ratios (HMOR_6.0, HMOR_9.8, HMOR_46) (■) and on chemically dealuminated MOR_9.8 samples with different Al contents (▲) [20 kPa DME, 930 kPa CO, 438 K].

the presence of H_2O concentrations that strongly inhibit carbonylation rates.

A mechanism involving competitive adsorption of CO and DME on the same type of site would lead to negative DME reaction orders, in contradiction with the measured zero-order kinetics in DME. Thus, CO bound competitively onto Brønsted acid sites cannot be the active species in carbonylation reactions. CO bound onto framework Al with methyl groups already bound would remove this inconsistency, as long as it occurred non-competitively (proposal (ii)); water inhibition of reactions of CO with CH_3 species would then reflect coordination of water to Al species vicinal to CH_3 groups, which interferes with the docking of active CO species.

Proposal (iii) would require CO binding on sites other than H^+ (e.g., Lewis acid sites that bind CO at low temperatures). Such sites may exist as extra-framework Al [49], but DME carbonylation rates (per total Al) did not change systematically with their concentration (Section 3.6; Figs. 10 and 11). CO binds on L_1-type Lewis acid sites with a heat of adsorption of $\sim$130 kJ/mol [44], which would lead to saturation of sites with CO surfaces during catalysis at 423 K and 1 MPa CO and thus to zero-order CO kinetic dependences. Similar arguments would render any CO species with detectable spectral features an unlikely candidate as a reactive intermediate. The ability of most and perhaps all CH_3 groups to form acetyl groups (Section 3.4; Fig. 5) indicates that sites that bind reactive centers are not minority species, because the reactivity of most CH_3 groups would require mobility of acetyls or CH_3 to place them near such minority sites. We have ruled out such mobility by showing that physical mixtures of HMOR_9.8 and HMFI_12.2 ($DME_{adsorbed}/Al_{total} = 0.5$) have similar carbonylation rates (per Al in HMOR_9.8) during transient CH_3-CO reactions; thus, sites in MOR cannot be used to carbonylate CH_3 groups on HMFI_12.2 sites located >1 μm away, as would have been expected for mobile acetyls or methyls.

The observed increase in rate with increasing H^+ content in MOR samples suggests that proximity of surface CH_3 groups (or trimethyloxonium) species increases carbonylation rates, perhaps because of a vicinal CH_3 group or merely because of the consequent implicit presence of a neighboring Al, leading to a more reactive CH_3 group. For random Al site distributions [50], this cannot explain differences in reactivity among MOR ($\sim$1 [mol g-atom^{-1} Al h^{-1}]), FER ($\sim$0.1 [mol g-atom^{-1} Al h^{-1}]), and MFI ($\sim$0.01 [mol g-atom^{-1} Al h^{-1}]) with similar Si/Al ratios. All zeolites give $DME_{adsorbed}/Al$ ratios of 0.5 ± 0.05; thus the proximity of CH_3 groups could not differ for random Al siting. The relative distribution of α, β, and γ sites from the UV–visible spectra of Co-exchanged materials (using methods described in Section 2.8) shows a predominance of β sites (>60%) in HMOR_9.8 and MFI_12.2 samples and no specific preference for α or γ sites for MOR or MFI materials [30–32], yet carbonylation rates on HMOR_9.8 and HMFI_12.2 catalysts differ by $\sim$100, indicating that rates do not change in parallel with the number of specific types of sites (α, β, γ). Alternatively, differences in reactivity may represent heterogeneity in CH_3 groups based on steric confinement in micropores for MOR samples with low Si/Al ratios versus CH_3 groups accessible via mesopores in dealuminated MOR materials with higher Si/Al ratios or via larger three-dimensional pore structures in MFI and USY. These specific requirements remain the subject of intense interest and additional studies within our group.

4. Conclusion

DME carbonylation occurs with high selectivity ($\sim$99%) on acidic mordenites at low temperatures (423–463 K) with first- and zero-order kinetic dependencies on CO and DME pressures, respectively. Induction periods are removed by pretreatment in DME because DME reacts initially with acidic protons to form methyl groups and methanol and/or water; the latter byproducts reversibly inhibit CO adsorption or reactions of CO with methyl groups to form acetyl intermediates in kinetically relevant steps. DME dissociative adsorption occurs reversibly to form surface methyl groups, and surface acetyl groups react with DME to re-form surface methyl groups during steps that lead to methyl acetate formation. Acidic mordenites with similar Si/Al ratios catalyze methyl acetate synthesis at varying rates. The concentrations of CO binding sites as measured by low-temperature IR and TPD studies in these materials did not correlate with DME carbonylation rates, and their low levels ($\sim$0.01 per Al) cannot justify the $\sim$55% excess methyl acetate/Al formed in transient reactions of DME and CO. Methyl acetate synthesis rates per Al increase with increasing proton concentration, suggesting that aluminum pair sites occupied by either methyl groups of Brønsted sites may be required for CO reactions with CH_3 groups or that CH_3 groups in sterically confined environments of low-silica mordenites may have higher reactivity for carbonylation.

Supplementary material

Supplementary material for this article may be found on ScienceDirect, in the online version.

Please visit DOI: 10.1016/j.jcat.2006.09.020.

Appendix A. Derivation for the kinetic equations described in Section 3.1

The concentrations of $^{*a}CO$ and $^{*a}H_2O$ are solved using quasi-equilibrium approximations in terms of $(^{*a})$, the concentration of unspecified CO binding sites,

$$\left(^{*a}CO\right) = K_1 P_{CO}\left(^{*a}\right)$$

and

$$\left(^{*a}H_2O\right) = K_2 P_{H_2O}\left(^{*a}\right).$$

$C_{T,a}$ is the sum of $(^{*a})$ and the concentration of the species bound to ^{*a},

$$C_{T,a} = \left(^{*a}\right) + \left(^{*a}CO\right) + \left(^{*a}H_2O\right)$$
$$= \left(^{*a}\right)(1 + K_1 P_{CO} + K_2 P_{H_2O}).$$

The concentration of $^{*a}CO$ becomes

$$\left(^{*a}CO\right) = \frac{K_1 P_{CO} C_{T,a}}{1 + K_1 P_{CO} + K_2 P_{H_2O}}.$$

The concentration of $^{*b}H$ in terms of $(^{*b}CH_3)$ is determined by the quasi-equilibrium approximation,

$$\left(^{*b}H\right) = \frac{P_{H_2O}(^{*b}CH_3)}{K_4 P_{CH_3OH}}.$$

The pseudo-steady-state approximation is used to solve for $(^{*b}COCH_3)$,

$$\frac{d(^{*b}COCH_3)}{dt} = k_5\left(^{*a}CO\right)\left(^{*b}CH_3\right) - k_6\left(^{*b}COCH_3\right)P_{DME} \approx 0,$$

$$\left(^{*b}COCH_3\right) = \frac{k_5(^{*a}CO)(^{*b}CH_3)}{k_6 P_{DME}},$$

and the sum of all species bound at Brønsted acid sites becomes

$$C_{T,b} = \left(^{*b}CH_3\right) + \left(^{*b}H\right) + \left(^{*b}COCH_3\right)$$
$$= \left(^{*b}CH_3\right)\left(1 + \frac{P_{H_2O}}{K_4 P_{CH_3OH}} + \frac{k_5(^{*a}CO)}{k_6 P_{DME}}\right).$$

The acetyl concentration is given by

$$\left(^{*b}COCH_3\right) = \frac{k_5(^{*a}CO)}{k_6 P_{DME}}\left(\frac{C_{T,b}}{1 + \frac{P_{H_2O}}{K_4 P_{CH_3OH}} + \frac{k_5(^{*a}CO)}{k_6 P_{DME}}}\right).$$

The rate of methyl acetate formation is

$$r_{CH_3COOCH_3} = k_6\left(^{*b}COCH_3\right)P_{DME},$$

which, after substitution, becomes

$$= \frac{K_1 k_5 P_{CO} C_{T,a}}{1 + K_1 P_{CO} + K_2 P_{H_2O}}$$
$$\times \left(\frac{1}{1 + \frac{P_{H_2O}}{K_4 P_{CH_3OH}} + \frac{K_1 k_5 P_{CO} C_{T,a}}{k_6 P_{DME}(1 + K_1 P_{CO} + K_2 P_{H_2O})}}\right).$$

In the presence of few surface-bound CO and the absence of H_2O, the rate of methyl acetate synthesis becomes

$$r_{CH_3COOCH_3} = K_1 k_5 P_{CO} C_{T,a}.$$

References

[1] G.J. Sunley, D.J. Watson, Catal. Today 58 (2000) 293.
[2] M.J. Howard, M.D. Jones, M.S. Roberts, S.A. Taylor, Catal. Today 18 (1993) 325.
[3] P.M. Maitlis, A. Haynes, G.J. Sunley, M.J. Howard, J. Chem. Soc. Dalton Trans. (1996) 2187.
[4] F.E. Paulik, J.F. Roth, Chem. Commun. (1968) 1578.
[5] J.F. Roth, J.H. Craddock, A. Herschman, F.E. Paulik, Chemtech (1971) 600.
[6] N. Yoneda, Y. Shiroto, K. Hamato, S. Asaoka, T. Maejima, US 5334755, 1994, Chiyoda.
[7] H. Koch, Fette Seifen Anstrichmittel 59 (1957) 493.
[8] A. Bagno, J. Bukala, G.A. Olah, J. Org. Chem. 55 (1990) 4284.
[9] H. Bahrmann, New Syntheses with Carbon Monoxide, Springer-Verlag, Berlin, 1980, p. 372.
[10] M.V. Luzgin, V.N. Romannikov, A.G. Stepanov, K.I. Zamaraev, J. Am. Chem. Soc. 118 (1996) 10890.
[11] M.V. Luzgin, A.G. Stepanov, A. Sassi, J. Sommer, Chem. Eur. J. 6 (2000) 2368.
[12] A.G. Stepanov, M.V. Luzgin, A.V. Krasnoslobodtsev, V.P. Shmachkova, N.S. Kotsarenko, Angew. Chem. Int. Ed. 39 (2000) 3658.
[13] A.G. Stepanov, M.V. Luzgin, V.N. Romannikov, V.N. Sidelnikov, K.I. Zamaraev, J. Catal. 164 (1996) 411.
[14] A.G. Stepanov, M.V. Luzgin, V.N. Romannikov, K.I. Zamaraev, J. Am. Chem. Soc. 117 (1995) 3615.
[15] T. Li, N. Tsumori, Y. Souma, Q. Xu, Chem. Commun. (2003) 2070.
[16] Q. Xu, S. Inoue, N. Tsumori, H. Mori, M. Kameda, M. Tanaka, M. Fujiwara, Y. Souma, J. Mol. Catal. A Chem. 170 (2001) 147.
[17] K. Fujimoto, T. Shikada, K. Omata, H. Tominaga, Chem. Lett. (1984) 2047.
[18] B. Ellis, M.J. Howard, R.W. Joyner, K.N. Reddy, M.B. Padley, W.J. Smith, Stud. Surf. Sci. Catal. 101 (1996) 771.
[19] W.J. Smith, United Kingdom 5420345, 1995, BP Chemicals Limited.
[20] A. Sardesai, S. Lee, T. Tartamella, Energ. Source 24 (2002) 301.
[21] G.G. Volkova, L.M. Plyasova, A.N. Salanov, G.N. Kustova, T.M. Yurieva, V.A. Likholobov, Catal. Lett. 80 (2002) 175.
[22] G.G. Volkova, L.M. Plyasova, L.N. Shkuratova, A.A. Budneva, E.A. Paukshtis, M.N. Timofeeva, V.A. Likholobov, Stud. Surf. Sci. Catal. 147 (2004) 403.
[23] R.W. Wegman, J. Chem. Soc. Chem. Commun. (1994) 947.
[24] P. Cheung, A. Bhan, G.J. Sunley, E. Iglesia, Angew. Chem. Int. Ed. 45 (2006) 1617.
[25] M.R. Apelian, A.S. Fung, G.J. Kennedy, T.F. Degnan, J. Phys. Chem. 100 (1996) 16577.
[26] M. Muller, G. Harvey, R. Prins, Micropor. Mesopor. Mater. 34 (2000) 135.
[27] A.P.M. Kentgens, K.F.M.G.J. Scholle, W.S. Veeman, J. Phys. Chem. 87 (1983) 4357.

[28] E. Iglesia, J. Baumgartner, G.L. Price, K.D. Rose, J.L. Robbins, J. Catal. 125 (1990) 95.

[29] G.L. Price, E. Iglesia, Ind. Eng. Chem. Res. 28 (1989) 839.

[30] J. Dedecek, B. Wichterlova, J. Phys. Chem. B 103 (1999) 1462.

[31] J. Dedecek, D. Kaucky, B. Wichterlova, O. Gonsiorova, Phys. Chem. Chem. Phys. 4 (2002) 5406.

[32] L. Drozdova, R. Prins, J. Dedecek, Z. Sobalik, B. Wichterlova, J. Phys. Chem. B 106 (2002) 2240.

[33] T.R. Forester, R.F. Howe, J. Am. Chem. Soc. 109 (1987) 5076.

[34] S.M. Campbell, X.Z. Jiang, R.F. Howe, Micropor. Mesopor. Mater. 29 (1999) 91.

[35] D. Lesthaege, V. Van Speybroeck, G.B. Marin, M. Waroquier, Chem. Phys. Lett. 417 (2006) 309.

[36] W. Wang, A. Buchholz, M. Seiler, M. Hunger, J. Am. Chem. Soc. 125 (2003) 15260.

[37] W. Wang, M. Seiler, M. Hunger, J. Phys. Chem. B 105 (2001) 12553.

[38] I.I. Ivanova, A. Corma, J. Phys. Chem. B 101 (1997) 547.

[39] R. Shah, J.D. Gale, M.C. Payne, J. Phys. Chem. B 101 (1997) 4787.

[40] N. Hartz, G. Rasul, G.A. Olah, J. Am. Chem. Soc. 115 (1993) 1277.

[41] O. Kresnawahjuesa, R.J. Gorte, D. White, J. Mol. Catal. A Chem. 208 (2004) 175.

[42] A. Zecchina, C.O. Arean, Chem. Soc. Rev. 25 (1996) 187.

[43] J.A. Lercher, C. Grundling, G. Eder-Mirth, Catal. Today 27 (1996) 353.

[44] L. Benco, T. Bucko, J. Hafner, H. Toulhoat, J. Phys. Chem. B 108 (2004) 13656.

[45] M.I. Zaki, H. Knozinger, Spectrochim. Acta A 43 (1987) 1455.

[46] H. Knozinger, P. Ratnasamy, Catal. Rev. Sci. Eng. 17 (1978) 31.

[47] S. Bordiga, C. Lamberti, F. Geobaldo, A. Zecchina, G.T. Palomino, C.O. Arean, Langmuir 11 (1995) 527.

[48] M. Maache, A. Janin, J.C. Lavalley, E. Benazzi, Zeolites 15 (1995) 507.

[49] M.A. Makarova, A.E. Wilson, B.J. van Liemt, C. Mesters, A.W. de Winter, C. Williams, J. Catal. 172 (1997) 170.

[50] B.R. Goodman, K.C. Hass, W.F. Schneider, J.B. Adams, Catal. Lett. 68 (2000) 85.